



Brain tumors induce immunoregulatory dendritic cells in draining lymph nodes that can be targeted by OX40 agonist treatment

Oscar Badillo-Godinez , Jenni Niemi, Liam Helfridsson, Shokoufeh Karimi, Mohanraj Ramachandran, Hitesh Bhagavanbhai Mangukiya , Sven Nelander, Mats Hellström

To cite: Badillo-Godinez O, Niemi J, Helfridsson L, *et al.* Brain tumors induce immunoregulatory dendritic cells in draining lymph nodes that can be targeted by OX40 agonist treatment. *Journal for ImmunoTherapy of Cancer* 2025;13:e011548. doi:10.1136/jitc-2025-011548

► Additional supplemental material is published online only. To view, please visit the journal online (<https://doi.org/10.1136/jitc-2025-011548>).

Accepted 29 April 2025



© Author(s) (or their employer(s)) 2025. Re-use permitted under CC BY-NC. No commercial re-use. See rights and permissions. Published by BMJ Group.

Department of Immunology, Genetics and Pathology, Uppsala University, Uppsala, Sweden

Correspondence to

Dr Mats Hellström;
mats.hellstrom@igp.uu.se

ABSTRACT

Background Primary and metastatic brain tumors have a poor prognosis, partly owing to the unique characteristics of the central nervous system (CNS) and tumor immune microenvironment (TIME). One distinct feature of the CNS TIME is the limited infiltration and activation of dendritic cells (DCs). The impact of CNS versus non-CNS TIME can be assessed by injecting tumor cells from the same model, either subcutaneously (peripherally) or into the brain. Subcutaneous tumors drain into the tumor-draining lymph nodes in the skin (TdLN-p), whereas brain tumors drain into the deep cervical TdLN (TdLN-c). We previously showed that CNS tumors that are not responsive to immune checkpoint inhibition become responsive when grown peripherally, and that non-responsiveness correlates with a tolerogenic immune response in the local TIME and TdLN-c.

Methods In this study, we investigated the immunoregulatory potential of cervical DCs (DC-c) compared with that of peripheral DCs (DC-p) using high-resolution flow cytometry, single-cell RNA sequencing, and ex vivo and in vivo functional characterization of TdLNs from mouse models of glioma and lymphoma.

Results Our analysis revealed that DC-c promoted regulatory T-cell expansion and poorly cytotoxic CD8⁺ T cells compared with DC-p. Furthermore, we identified OX40 (*Tnfrsf4*) as a modulator of immunoregulatory DC-c function and found that its antitumor effect depended on lymphocyte trafficking and the DC transcription factor *Batf3*. CCR7+OX40+ DCs were efficient in antigen processing and presentation, and OX40 agonists further enhanced DC activation. In TIME, the CCR7+OX40+ DCs expressed OX40L, and blocking it promoted Treg formation ex vivo.

Conclusions Our findings highlight the unique immunoregulatory functions of DC-c in TdLNs and suggest the importance of OX40 signaling through direct effects on CCR7+OX40+ DCs and indirect effects on T cells.

BACKGROUND

Primary or metastatic central nervous system (CNS) malignancies are associated with poor prognosis, irrespective of the cancer type.^{1,2} In addition, the efficacy of immunotherapeutic

WHAT IS ALREADY KNOWN ON THIS TOPIC

⇒ Dendritic cells (DCs) from cervical tumor-draining lymph nodes (TdLN-c) play a role in initiating immune responses to brain tumors. However, the phenotype and function of DCs in TdLN-c compared with those in TdLN associated with tumors outside the brain have not been thoroughly characterized.

WHAT THIS STUDY ADDS

⇒ This study demonstrates that DCs in TdLN-c are tolerogenic and exhibit distinct phenotypic markers compared with DCs from skin TdLN. The composition of DC subtypes is also unique, with a higher proportion of DC2s in TdLNs-c than in peripheral TdLNs. Importantly, OX40 signaling can reprogram the tolerogenic environment of TdLN-c by activating OX40+CCR7+ DCs and T cells, ultimately eliciting a therapeutic immune response.

HOW THIS STUDY MIGHT AFFECT RESEARCH, PRACTICE OR POLICY

⇒ Reprogramming CCR7+OX40+ DCs through OX40 stimulation offers a potential strategy to overcome immune suppression in brain tumors. This approach, combined with other immunomodulatory strategies, could enhance antitumor responses and inform the design of novel immunotherapies and clinical trials for brain tumor treatment.

strategies such as immune checkpoint inhibitors (ICIs) is low in patients with brain metastasis.^{3–7} Improving dendritic cell (DC) stimulation can enhance antitumor immunity in CNS malignancies, owing to their low presence in the CNS.^{8,9} Tumor-infiltrating DCs have been characterized based on their marker expression, particularly in peripheral tumors.^{10–14} Single-cell RNA sequencing (scRNA-seq) across DC populations has revealed shared gene and protein expression patterns, highlighting conserved traits across species despite tumor heterogeneity.^{15–17} This analysis identified two additional subsets, DC3

and mature regulatory DC (mregDC), with properties associated with an inflammatory or immunoregulatory signature, respectively, correlating with a favorable prognosis for immunotherapy response.^{15,16} Adjuvant ICI treatment using an anti-programmed death 1 (PD-1) treatment in patients with glioblastoma results in the expansion of infiltrating CD8⁺ T cells and the induction of costimulatory molecules in glioma cDC1s. Furthermore, data from a phase III clinical trial in GBM using an autologous tumor lysate vaccine with DCs suggest a prolonged overall survival.^{18–20} In human patients with brain melanoma and leptomeningeal metastases, the presence of the DC3 subtype correlates with improved overall survival. Similarly, in mouse models, the presence of DC3 is associated with an enhanced response to programmed death 1 (PD-1) blockade.²¹ This suggests that the presence of different DC subtypes is important for patient outcomes and can be affected by treatment. However, tumor-draining lymph nodes (TdLNs) are important in the cancer immunity cycle,²² and the specific DC subtypes present in the TdLN or the tumor immune microenvironment (TIME) of the brain, as well as their relationship to DCs in other areas, remain unclear.

In this study, we characterized the phenotype and function of cervical DCs (DC-c) compared with peripheral/subcutaneous DCs (DC-p) in TdLN using two tumor models from glioma and lymphoma and compared the findings from subcutaneous and intracranial tumors.

This revealed that DC-c promoted the induction of Tregs and reduced cytotoxic CD8⁺ T-cell responses, irrespective of the tumor type. Combined antibody and RNA sequencing revealed six DC subtypes: DC1, DC2, XCR1+DC, CCR7+DC, plasmacytoid DC (pDCs), and immature DC (imDC), with a high prevalence of DC2 in cervical TdLN (TdLN-c) and an increased number of CCR7+DC in TdLN-p. Treatment with an OX40 agonist overcame the regulatory DC-c functions, and the response depended on the transcription factor *Batf3* and lymph node (LN) trafficking. Further analysis showed that OX40 was present on pDC as well as CCR7+DC in the TIME and ex vivo samples, and OX40 agonist induced activation of CCR7+OX40 DCs ex vivo. Of the two OX40+DC populations, only CCR7+DCs depended on *Batf3*. This suggests that the TIME and TdLN of brain tumors contain immunoregulatory DCs, and OX40 stimulation can overcome the impact of these immunoregulatory DCs by directly acting on CCR7+OX40+ DCs and most likely on OX40+T cells. These findings provide critical insights into the role of DC subtypes in brain tumor immunity and highlight a promising strategy to enhance antitumor immune responses by targeting specific immunoregulatory functions in TdLN-c.

METHODS

Cell lines

SB28-parental cells expressing luciferase and GFP were cultured as previously described²³ in DMEM supplemented with 10% FBS, 2 mM glutamine, 100 U/mL penicillin, and 100 mg/mL streptomycin (Gibco). The SB28-OVA cell line was cultured with 400 µg/mL G418

(Gibco). EG7-OVA cells were cultured in RPMI supplemented with 10% FBS, 50 µM 2-ME, 400 µg/mL G418, and 2 mM glutamine.

Mouse studies

Female C57BL/6 mice, aged 6–8 weeks, were obtained from Taconic. Transgenic OT-I, OT-II C57BL/6-Tg, and *Batf3*^{tm1Kmm/J} mice were acquired from Charles River. All experiments were conducted according to the ARRIVE1 reporting guidelines²⁴ and national guidelines and regulations (permit: 5.8.18-14723/2020).

Orthotopic murine glioma models

To induce orthotopic brain tumors, 1.600 SB28-parental, SB28-OVA, or 25.000 EG7-OVA cells were injected intracranially (i.c.). The mice were anesthetized with isoflurane, and a burr hole was drilled in the skull, positioned 1.5 mm laterally anteroposterior and 1.5 mm mediolaterally to the bregma. A non-coring needle (Hamilton7804-04, 26-gage) was injected into the brain at a depth of 3 mm. Mice were administered carprofen (0.05 mg/kg) intraperitoneally (i.p.) immediately following surgery. Prior to imaging, mice were injected i.p. with 15 mg/kg luciferase (AAT Bioquest115144-35-9). The signal was analyzed using an IVIS Lumina III Perkin Elmer.

Murine subcutaneous tumor models

Mice were subcutaneously (s.c.) injected in the flank with 5×10⁵ tumor cells resuspended in phosphate-buffered saline (PBS). Tumor size was measured 1–2 times weekly, and the volume was calculated using the following formula: (length×width²)/2.

For in vivo treatment, mice were treated i.p. with 200 µg αOX40 agonistic antibodies (OX-86) or IgG control (BioXCell) on days 4, 7, and 10 post-tumor inoculation. The mice were monitored daily, evaluated for tumor-related symptoms, and euthanized using CO₂ at the humane endpoint. Mice were sacrificed on day 12 post-tumor injection to collect TdLNs for ex vivo experiments, scRNA-seq, and flow cytometry.

Mice were injected i.p. with 25 µg of FTY720 (APExBIO) on the day the treatment began and received maintenance doses of 20 µg every other day until day 16 post-tumor inoculation.

Harvesting of LNs

The cervical or inguinal LNs were harvested and placed in fresh RPMI, incubated for 10 min at 37°C with Liberase (250 µg/mL) and DNase (50 µg/mL Merck) and passed through a 70 µm cell strainer. Splenocytes were harvested and incubated with RBC lysis buffer (Invitrogen).

DCs from the LN or OT cells from the spleen were resuspended in MACS buffer with anti-CD4, anti-CD8 Microbeads or Pan Dendritic Cell Biotin-Antibody Cocktail (Milteny Biotec, Lund, Sweden), according to the supplier's instructions.

Ex vivo experiments

OT cells were incubated with 5 μ M of green CellTrace (Thermo Scientific, Bleiswijk, Netherlands), cultured in 96-well plates with 50 \times 10³ 1:1 OT-I:II cells, and co-cultured with 5 \times 10³ TdLN DCs.

The following stimuli were added: Poly-I:C 5 μ g/mL (Adipogen Life Sciences), α CD40 (FGK45), α IL-6 (MP5-20F3), α IL-4 (BVD6-24G2), α OX40 (OX-86), α CD200 (OX-90), and α PDL-1 (10F.9G2TM) (BioXcell) at a concentration of 100 ng/mL. In parallel, OT cells were cultured with DCs from cervical LNs (DC-c) and mixed at ratios of 1:1, 10:1, or 1:10 with subcutaneous/peripheral DCs (DC-p) at a final concentration of 5 \times 10³. OVA peptide H-2Kb SIINFEKL, 323-339 OVA I-Ab (Merck), and control peptides H-2Kb glycoprotein BSSIEFARL (TS-M523-PMBL) and HBc 128-140 TPPAYRPPNAPIL (TS-M701-PMBL) were added at a concentration of 10 μ g/mL and incubated for 5–7 days. To evaluate antigen uptake, DCs were first incubated with 10 μ g/mL OVA-DQ (with or without α OX40, Poly-I:C, α OX40L, or control IgG) at 37°C, and 30 min later, cells were washed and regular medium was added. After 3 hours of incubation, cells were collected and washed with cold PBS containing 2% FBS. Fluorescence was monitored using flow cytometry. For antigen presentation, pulsed DCs were co-cultured with OT cells as described above.

Single-cell library preparation and sequencing

Single-cell libraries were prepared using the BD Rhapsody platform (BD Biosciences) as previously described.²⁵ TdLN single-cell suspensions were labeled using a mouse single-cell sample multiplexing kit (#633793) and BD AbSeq-Oligos α CD11b (#940008,M1/70), α CD200 (#940208,OX90), α F4/80 (#940131,T45-2342), and α CD103 (#940136,M290). The pooled samples were loaded onto a BD Rhapsody cartridge (#633733), and mRNA was captured according to the manufacturer's protocol (#633731). Targeted cDNA libraries of genes in the BD Rhapsody Immune Response Panel Mm (#633753) supplemented with additional genes (online supplemental table 1), along with sample tags and BD AbSeqs, were prepared using the BD Rhapsody Targeted mRNA and AbSeq Amplification kit (#633774). The final libraries were sequenced (Read1:51 bp, Read2: 71 bp+i7 Indexes: 8bp) on a NovaSeq6000 S Prime sequencer (Illumina, San Diego, California, USA) on the SNP&SEQ Technology Platform (Uppsala, Sweden).

Analysis of scRNA-seq data

Fastq files were processed on Seven Bridges using the Rhapsody Analysis Pipeline (BD Biosciences). Recursive substitution Error Correction (RSEC) and Distribution-Based Error Correction algorithms developed by the manufacturer (BD Biosciences) were used. Cells that did not meet the criteria for singlets or multiplets were classified as undetermined. The final read depths for the library were as follows: mRNA, 72,938.31; average reads/cell, 99.72% sequencing saturation; AbSeq, 1,968.14; average

reads/cell, 88.12% sequencing saturation, which were within the expected range of the manufacturer's recommendations for targeted transcriptomic sequencing.

Single-cell sequencing analysis workflow

Data analysis was performed using Partek Flow build V.10.0.21.0411 (Partek, St. Louis, Michigan, USA). RSEC-adjusted molecular counts were used, and undetermined cells, multiplets, and cells with <50 detected transcripts were excluded. Data were normalized as counts per 10 000 with an offset of one count, and Log2 transformation was performed as recommended by the manufacturer (BD Biosciences) using the data normalization module in Partek Flow. Dimensionality reduction was performed using principal component analysis (PCA) followed by uniform manifold approximation and projection (UMAP). Clustering was performed using the Louvain clustering algorithm (nearest neighbor type: NN-Descent, number of nearest neighbors: 30), and biomarkers for each cluster were computed using analysis of variance tests with Benjamini-Hochberg correction for false discovery rate values ≤ 0.05 , and log2 fold change ≥ 1.5 .

Immunofluorescence staining, tumor-infiltrating lymphocyte extraction and flow cytometry

The relevant details are described in online supplemental information and online supplemental table 2.

RESULTS

TdLNs exhibit distinct immunophenotypes depending on the tumor site

We previously reported that the immune response in cervical (TdLN-c) differs from that in peripheral TdLN (TdLN-p).²³ To further investigate T-cell responses, we characterized TdLN-c or TdLN-p either i.c. or s.c. on day 12 post-tumor inoculation of ovalbumin (OVA) expressing SB28 mouse glioma cells (SB28-OVA) (figure 1A). Analysis of individual T-cell populations indicated an increase in the percentage of Tregs in TdLN-c (figure 1B and online supplemental figure 1A), whereas TdLN-p exhibited a high percentage of central and effector memory CD8+T cells (figure 1C). Both TdLNs had equal numbers of exhausted T cells expressing PD-1+and TIM-3+ (figure 1D). We evaluated the expression of killer cell lectin-like receptor G1 (KLRG1), expressed in a population that has lost the ability to proliferate and induce a memory T-cell response.²⁶ TdLN-p showed higher expression of long-term memory proteins in CD8+T cells (KLRG1-CD127+CD44+) than TdLN-c, which exhibited a short-term memory profile (KLRG1+CD127+CD44+) in CD4+T cells (figure 1E).

To confirm that the altered T-cell profile was not dependent on antigen load, we harvested TdLNs and restimulated the cells. Under the same conditions, TdLN-c cells maintained a high percentage of Tregs (figure 1F and online supplemental figure 1B). In contrast, TdLN-p was less regulated and exhibited a cytotoxic profile

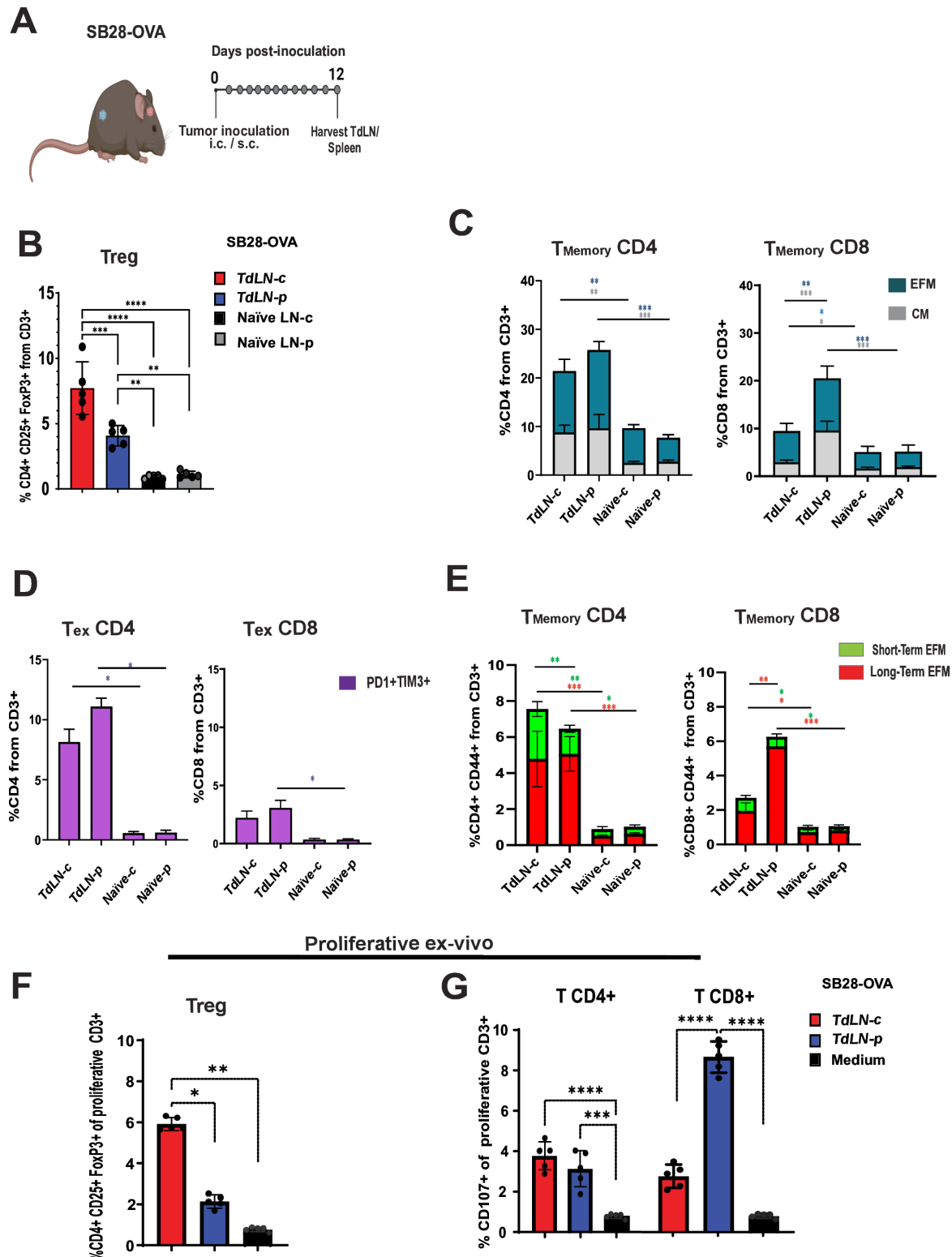


Figure 1 Tumor site-dependent immunological profile of tumor-draining lymph nodes (TdLN). (A) Schematic representation of the experiment: mice were inoculated with SB28-OVA intracranially (i.c.) or subcutaneously (s.c.). On day 12 post-tumor inoculation, TdLNs were harvested. (B) Quantification of regulatory T cells (Tregs) presented as the percentage of CD4+CD25+ FOXP3+ cells out of the total CD3+ counts. (C) Memory T-cell subsets are defined as effector memory (EFM: CD44+CD62L-) and Central Memory (CM: CD44+CD62L+) T cells. (D) Exhausted T cells identified by the expression of PD-1/TIM3. (E) Long-term memory (CD44+CD127+ KLRG1-) and short-term memory (CD44+CD127+ KLRG1+). (F, G) Mice were inoculated with SB28-OVA i.c. or s.c., and TdLNs were harvested on day 12 after tumor inoculation. The bulk cells were stained with green CellTrace, cultured in the presence of OVA peptides for 48 hours, and proliferative cells were analyzed. Tregs (percentage CD4+CD25+ FOXP3+) (F) and cytotoxic T cells (CD107+) (G) were evaluated. Graphs display mean \pm SD; analysis was conducted using a two-way ANOVA with Tukey's correction. * $p < 0.05$, ** $p < 0.01$, *** $p < 0.001$, **** $p < 0.0001$. ANOVA, analysis of variance.

(figure 1G). We observed an increase in the T-cell exhaustion profile of TdLN-p (online supplemental figure 1C).

These results indicate that TdLN-c induces a regulatory T-cell profile, whereas TdLN-p possesses a high T-cell memory with a long-term profile, particularly in CD8+T cells.

TdLN-c DCs exhibit a more regulatory T-cell profile in both glioma and lymphoma models as compared with DCs from TdLN-p

As DC subtypes play specific roles in activation and function, potentially contributing to the antitumor response to treatment, we investigated differences in the TdLN DCs population between subcutaneous and intracranial SB28-OVA tumors. DCs were defined as MHCII+CD11c+Ly6c[−]CD24+F4/80[−]^{27 28} (online supplemental figure 2A). We analyzed migratory (CD103+CD8⁺), resident (CD103-CD8⁺) DC1,²⁹ and CD11b+CD8[−] DC2³⁰ and observed a shift in the proportion of DC1 compared with DC2 from TdLN-p to TdLN-c, where CD8+CD103⁺ cells in TdLN-p were higher (figure 2A). To determine whether this profile was related to tumor type or LN location, we used cells from a lymphoma model (EG7-OVA) injected s.c. or i.c., which revealed a similar profile with an increase in DC1 in TdLN-p compared with TdLN-c (figure 2B).

Under normal conditions, naïve DCs exhibit low expression of activation markers. We observed that DC-c and DC-p from TdLN upregulated CD40 and CD86 on tumor challenge compared with naïve DCs. In addition, CD40 expression on DC2-p cells was significantly increased compared with that on DC2-c cells; CD86 expression was also upregulated in DC2-p cells in the EG7 model (online supplemental figure 2B,D). To determine whether this profile was specific to TdLNs or arose from a systemic response, we examined the DC profile of the spleen. Minimal changes were observed in the spleen, suggesting that the tumor response was prominent in the TdLNs (online supplemental figure 2E). We assessed antigen presentation based on H-2Kb/SIINFEKEL+staining of both CD8+CD103⁺ and CD103[−] populations (figure 2C,E and online supplemental figure 2C). DC-c exhibited a reduction in antigen presentation compared with DC-p in both tumor models. In contrast, MHC-II expression remained unchanged in the DCs (online supplemental figure 2F). We used MHC-OVA tetramers to evaluate antigen-specific T cells. In both tumor models, we observed a higher percentage of tumor antigen-specific Tregs in TdLN-c than in TdLN-p (figure 2D,F). Conversely, TdLN-p exhibited an increase in antigen-specific memory T cells compared with TdLN-c in both models (online supplemental figure 2G,H).

In conclusion, DCs in TdLN-c exhibited lower antigen presentation in the context of MHC-I, more prominent induction of antigen-specific Treg profiles, and fewer memory T cells than those in TdLN-p.

DCs from TdLN-c drive a Treg response

To functionally study DCs, we performed ex vivo analysis of DCs enriched through negative selection and co-cultured them with green CellTrace-stained ovalbumin-specific T cells and OT cells in the presence of OVA peptides (figure 3A and online supplemental figure 3A). SB28-OVA TdLN DC-c cells had a greater propensity to induce Tregs than naïve or TdLN DC-p cells. DC-c stimulated only half of the cytotoxic CD8+T cell response compared with DC-p (figure 3B). For the EG7-OVA model, we observed a similar trend, even though the regulatory profile was more prominent in the SB28-OVA model (figure 3C). To confirm that this effect depended on DCs, we used *Batf3*-deficient mice lacking DC1 and treated them similarly. *Batf3*-deficient mice showed reduced induction of Treg or T-cell responses compared with naïve DCs (online supplemental figure 3A,B).

To determine the dominance of Treg induction in relation to DC-c or DC-p, we harvested TdLN-c and TdLN-p DCs, mixed them in defined ratios (1:1, 1:10, and 10:1), and cultured them. Compared with DC-c and DC-p cultured at a 1:1 ratio, the increase in DC-c (10:1) induced more Tregs, whereas the addition of DC-p (10:1) did not reduce the number of Tregs from the 1:1 baseline. This suggests a dose-response relationship between DC-c and the capacity to induce Tregs, which cannot be balanced by DC-p. This effect was more prominent in SB28-OVA mice than that in EG7-OVA mice (online supplemental figure 3C,D).

Given the tolerogenic profile of DC-c, we enhanced their functionality using various stimuli that act as immunomodulators of DC activation, namely a TLR3 agonist and a CD40 agonist for activation, TIME modulators such as IL-6, agents targeting regulatory markers such as CD200, strategies targeting specific subpopulations such as mregDCs with anti-IL-4, and an OX40 agonist to directly inhibit Treg formation.^{15 31–33} While all simulations affected the downregulation of Tregs for DC-c, only the OX40 agonist and poly-I:C induced cytotoxic T cells from TdLN-c (figure 3D). For DC-p, the anti-OX40 agonist, anti-CD200 antagonist, and anti-IL-6 antagonist showed a decrease in Tregs; however, the stimuli resulted in a reduction in the cytotoxic profile (figure 3E).

These findings suggest that DCs can stimulate diverse responses in TdLN-c and TdLN-p. Specifically, DC-c plays a dominant role in inducing Tregs, thereby hindering cytotoxic responses that can be overcome by poly-I:C or agonistic OX40 ex vivo. We further explored the OX40 agonistic antibody, as we previously explored poly-I:C in the SB28 model.²³

Reprogramming the DC profile in TdLN enhances antitumor response

In mice carrying SB28-OVA tumors, we observed that agonistic antibody OX40 stimulation affected the immune profile of TdLN-c, with increased antigen presentation by DC1-c (figure 4A,B and online supplemental figure 4A). Moreover, the OX40 agonist induced an increase

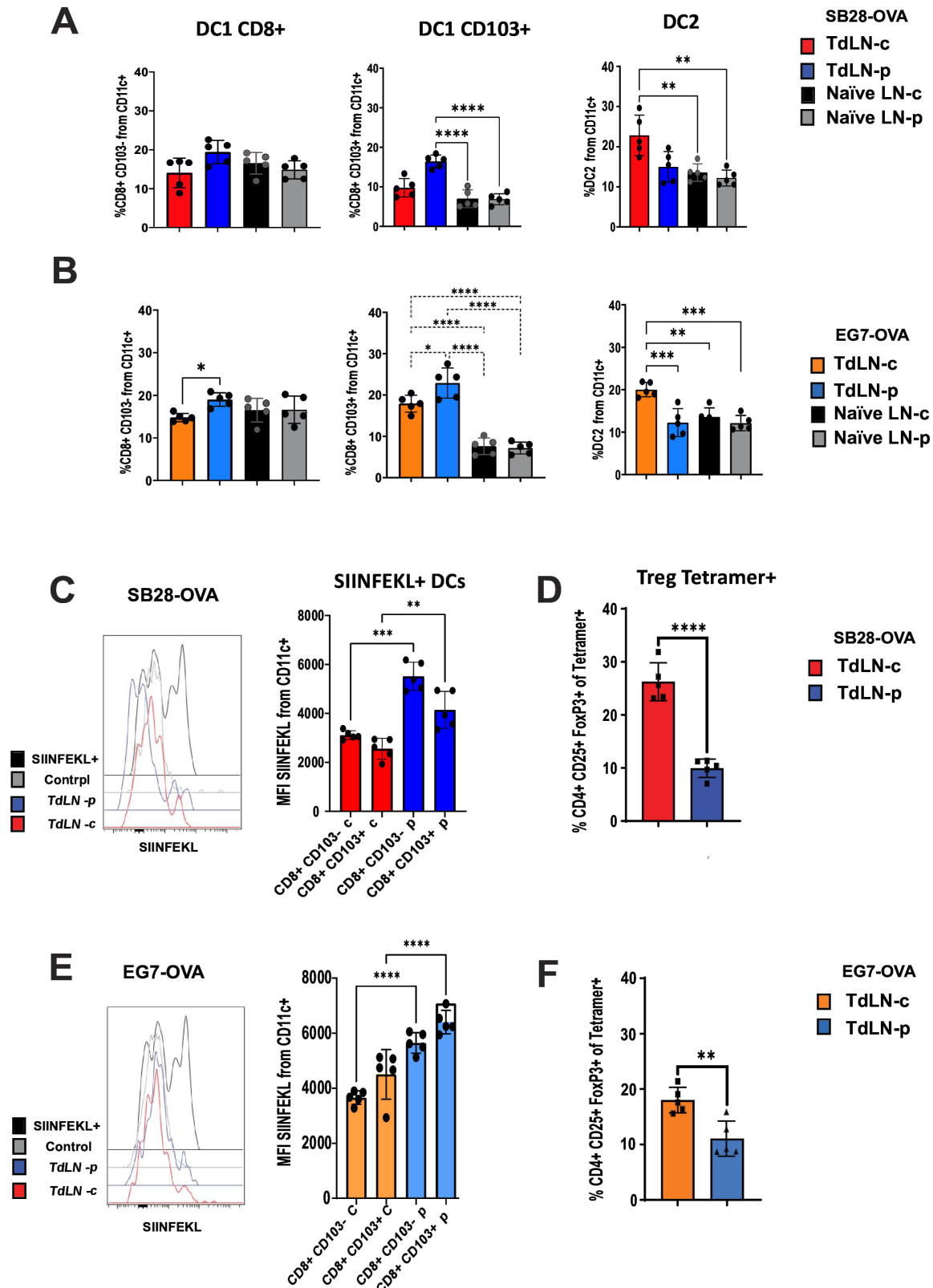


Figure 2 Cervical tumor-draining lymph nodes (TdLNs-c) have fewer antigen-presenting dendritic cells (DCs) with tolerogenic function, regardless of the brain tumor type, compared with TdLN-p. The mice were inoculated, as shown in figure 1. TdLNs were harvested at 12 days postinoculation. Quantification of DCs subtypes: DC1 (percentage CD8+CD103+ or CD8+ CD103-) and DC2 (CD11b+CD103-) in SB28-OVA tumors (A) and EG7-OVA tumor models (B). (C, E) Display the median fluorescence intensity (MFI) of DCs SIINFEKL+ in SB28-OVA and EG7-OVA tumor models, respectively. (D, F) Quantification of tetrameric OVA+regulatory T cells (CD4+CD25+ FOXP3+) in SB28-OVA and EG7-OVA tumor models, respectively. Graphs display mean±SD; statistical analysis was conducted using two-way ANOVA with Tukey's correction or unpaired t-test. *p<0.05, **p<0.01, ***p<0.001, ****p<0.0001. ANOVA, analysis of variance.

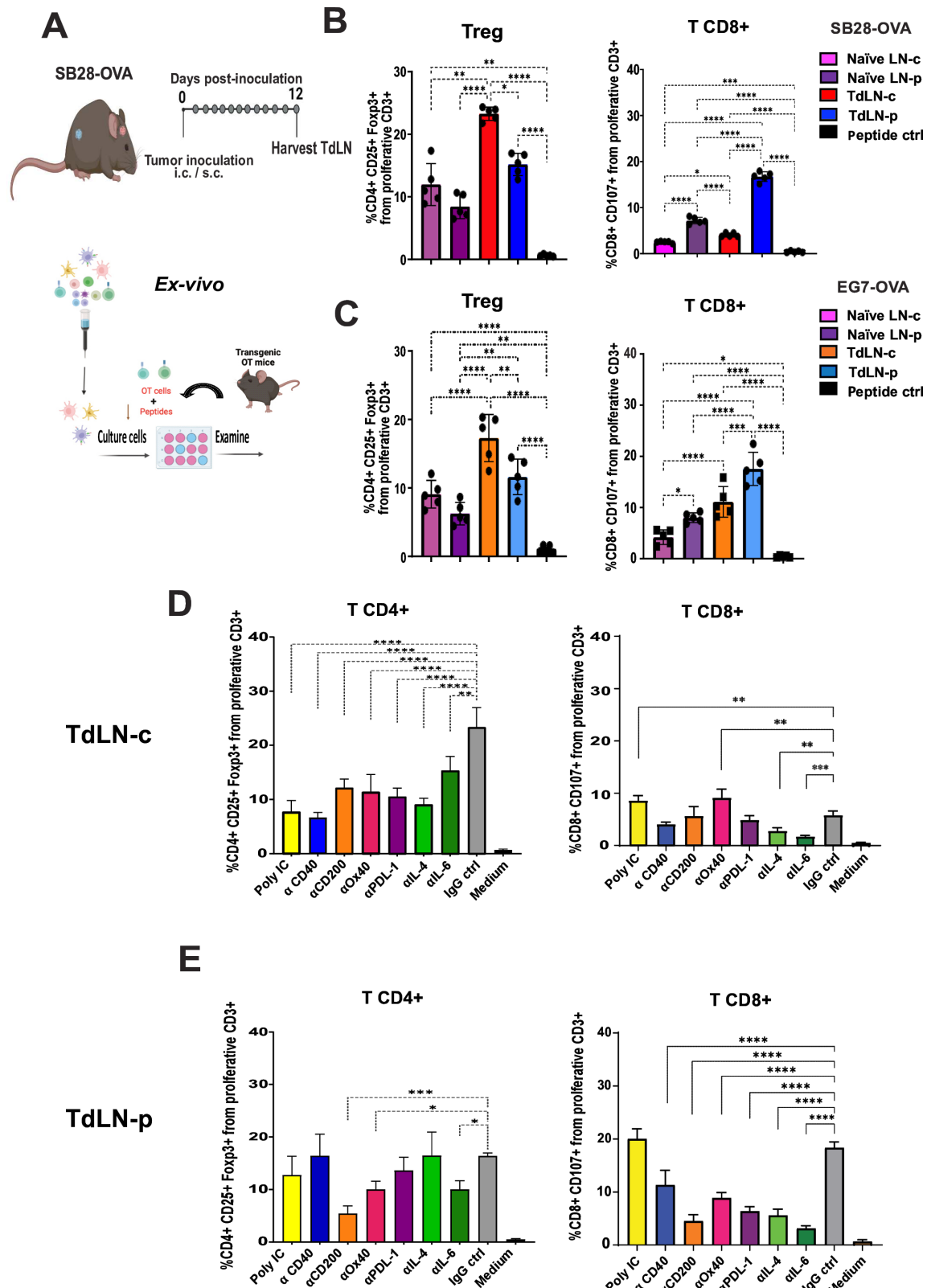


Figure 3 Reprogramming of tumor-draining lymph nodes (TdLN) dendritic cells (DCs) enhances the T-cell response. (A) Schematic representation of experimental procedures: For ex vivo culture, mice were inoculated i.c. or s.c. On day 12 post-tumor inoculation, TdLNs were harvested, and DCs were enriched and co-cultured with prestained OT cells with green CellTrace in the presence of OVA peptide. The percentage of Tregs (CD4+CD25+ Foxp3+) and Cytotoxic T cells CD8+ (CD107+) on SB28-OVA (B) or EG7-OVA (C) was calculated. Different stimuli were evaluated in ex vivo culture, and the percentages of Tregs, cytotoxic T cell CD8+ in TdLN-c (D) or TdLN-p (E) were calculated. Non-specific peptides and IgG isotypes were used as controls (n=5–7 mice/group). Statistics: Bar graphs show means±SD, two-way ANOVA with Tukey's correction, *p<0.05, **p<0.01, ***p<0.001, ****p<0.0001. ANOVA, analysis of variance; i.c., intracranially; s.c., subcutaneously.

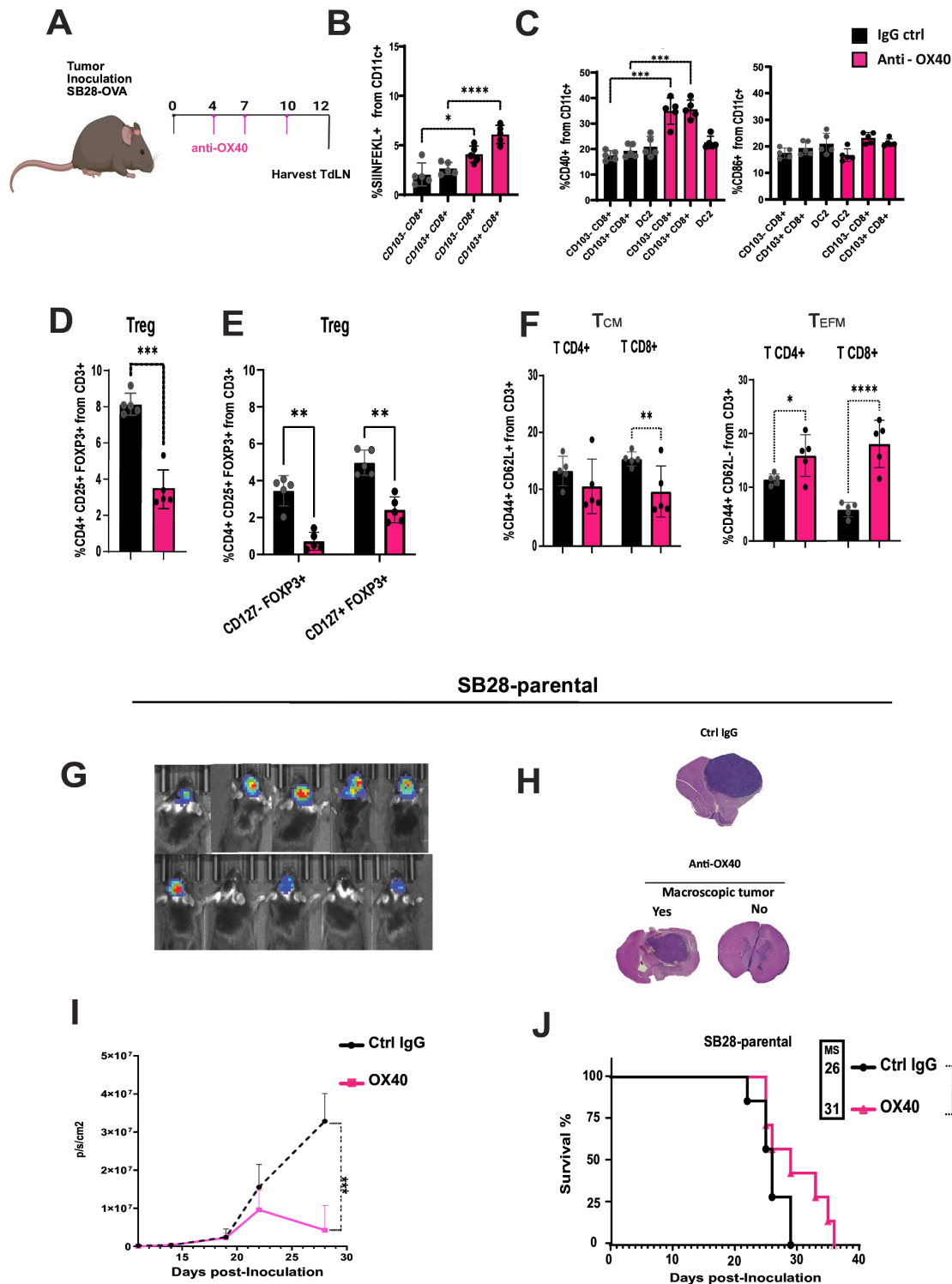


Figure 4 Treatment with an anti-OX40 agonist enhances immune responses in cervical TdLN. Schematic illustration of the experimental layout (A) used to obtain data shown in (B–F): groups of 5–7 mice were inoculated with the glioma cell line SB28-OVA, followed by i.p. administration of either an anti-OX40 agonist or IgG control on days 4, 7, and 10 post-tumor inoculation. On day 12 post-tumor inoculation, the TdLN-c were harvested, and single-cell suspensions were collected for immune profile analysis using flow cytometry. (B) H2b-SIINFEKL-positive DCs in TdLN on day 12 after treatment with OX40 agonist or control antibody. (C) Activation markers, CD40 and CD86, expressed by DCs. (D) Regulatory T cells (CD4+CD25+ Foxp3+). (E) Regulatory T cell (CD127+/-). (F) Memory T-cell response for CD4+ and CD8+ central memory (CM, CD44+CD62L+) and effector memory (EFM, CD44+CD62L-). (G, I) Tumor growth was evaluated using bioluminescence imaging. (H) H&E staining of brain tissue from the endpoint. (J) Kaplan–Meier survival curves of tumor-bearing mice treated with OX40 agonist or control IgG. The graph shows combined survival curves obtained from two independent experiments. Bar graphs show the mean±SD. One-way ANOVA multiple comparisons test *p<0.05, **p<0.01, ***p<0.001, ****p<0.0001. ANOVA, analysis of variance; i.p., intraperitoneally; TdLN, tumor-draining lymph nodes.

in CD40 expression in both DC1 subsets, whereas there was no change in the expression of CD86 compared with the control (figure 4C). In contrast, no changes were observed in the activation markers of DC2. OX40 treatment decreased the expansion and induction of CD127 positive (activated) and negative Tregs³⁴ (figure 4D,E). Memory T cells (figure 4F), particularly CD8+T cells, had a long-term profile (online supplemental figure 4B) that was enriched following OX40 agonist treatment. Furthermore, OX40-treated mice exhibited an exhausted T-cell profile compared with the control (online supplemental figure 4C).

The OX40 agonist treatment was also performed in mice injected with an SB28-parental cell line that did not express ovalbumin. We observed a 50% reduction in bioluminescence following OX40 agonist treatment and an extension in the median survival to 31 days compared with the control group at 26 days (figure 4G–J). In parallel, we analyzed tumor-infiltrating lymphocytes (TILs) 22 days postinoculation, immediately before the mice displayed symptoms. The OX40 agonist-treated mice exhibited a substantial reduction in proliferative Tregs and a corresponding increase in proliferating cytotoxic CD8+T cells (online supplemental figure 4D,E).

Endpoint analysis of TILs from treated mice showed that they maintained a cytotoxic and proliferative response, with fewer Tregs, regardless of tumor growth (online supplemental figure 4F,G).

We hypothesized that overactivation of the immune response could limit survival in a fraction of OX40 agonist-treated mice with low bioluminescence, but they still died. To confirm this, we explored the use of low-dose dexamethasone, a potent corticosteroid administered to patients with brain tumors, to reduce tumor-associated inflammation and edema.³⁵ Combination treatment with dexamethasone significantly increased the median survival (42 days), resulting in a survival rate of 12.5%, with no effect in the control-treated cohort (online supplemental figure 4H,I).

Collectively, these findings demonstrate that OX40 stimulation has the potential to reprogram the TIME and DC-c, enhance antigen presentation and activation, improve T-cell response, and lead to tumor response.

DC subpopulations from c-TdLN exhibit distinct mRNA expression profiles

Given the distinct functional differences between DC-c and DC-p, we analyzed DC subpopulations using scRNA-seq. Our analysis revealed six distinct clusters (figure 5A). Genes expressed in DC1 included *Cd8a*, *Irf8*, and high CD103 showed high expression, whereas DC2 expressed high levels of *Itgam*, *Irf4*, and CD11b. The pDCs expressed *Klra17*, *Fcer1g*, *Il7r*, and *Tlr7*, whereas imDCs had a low expression of MHC class II and expressed *Cd9*, *Xbp1*, and *Ifitm2* (online supplemental table 3).

We identified a cluster of cells closely related to DC1 in UMAP characterized by the expression of high *Cd8a*, *Irf8*, *Itgax* (CD11c), and *Xcr1*, along with intermediate

CD103 and the presence of activation genes, such as *Cd40* and *Cd86*. This suggests that they are similar, yet distinct from DC1 (referred to as XCR1+DCs). A cluster of cells near the DC2 cluster is referred to as CCR7+DCs. This cluster expresses the migration-associated gene *Ccr7* and, importantly, *Tnfrsf4* (OX40). In addition, the cluster expressed activation genes such as *Cd40* and *Cd63*, along with immunoregulatory genes such as *Cd274* and *Aldh1a2* (figure 5B,C).

Next, we conducted Gene Set Enrichment Analysis and Ingenuity Pathway Analysis by comparing DC-c and DC-p clusters, revealing that DC-p exhibited a significant overrepresentation of genes involved in the immune response pathways compared with DC-c (online supplemental figure 5A,B, online supplemental table 4). On intracluster analysis, DC1-c displayed upregulation primarily of *Itgae* (CD103) and a trend toward less *Cd8* than DC1-p. This observation was corroborated by flow cytometry results, which were consistent with the RNA data (online supplemental figure 5C). Moreover, the DC2-c cluster exhibited high expression of *S100a8*, *Gzmb*, and *Cpa3*, along with downregulation of *Jchain*, *Iglc3*, *Ltb*, and *Cd200*. Furthermore, the CCR7+DCc cluster primarily upregulated *Ifitm3* and *Btla* and downregulated *Arg2*, *Cxcl1*, and CD11b. The XCR1+DCc cluster displayed upregulation of *Ccl2* and *Bcl2a1a* and downregulation of *Elane*, *Cd34*, and *Ccl9* compared with XCR1+DCp. In the pDC cluster, *Lag3*, *Tnf*, and *Ifitm3* were upregulated in pDC-c, whereas *Il7r*, *Fosb*, *Vegfc*, and *Jchain* were downregulated in pDC-p. Notably, all DC-c clusters exhibited an increase in the expression of *Irf7* (online supplemental figure 5B). *Tnfrsf4* (OX40) mRNA was most highly expressed in the CCR7+DC cluster (figure 5C).

We evaluated the populations corresponding to the gene expression clusters using flow cytometry gating on CCR7+DC, CD11b (DC2), XCR1+DC, CD8/CD103 (DC1), and Ly6c/B220 (pDC) (online supplemental figure 5D). This confirmed the differential expression of activation (CD40, CD86, and CD63) and regulatory (PD-L1) markers, OX40, and OX40L (figure 5D,E). CCR7+DCs showed the highest expression levels of CD40, CD86, and OX40. OX40 protein was also expressed in the pDC subpopulation, and PDL1 was higher in DC2, CCR7+, and pDC than in DC1 and XCR1+DC, consistent with the RNA expression data (online supplemental figure 5E).

The proportion of DC populations differed between TdLN-c and TdLN-p. The DC2 population increased in TdLN-c in both models compared with that in TdLN-p (figure 2A,B). Unique to the SB28 model was the decrease in CCR7+DC in TdLN-c compared with TdLN-p and a decrease in XCR1+DCc compared with DC-p for the EG7-OVA. Knockout of *Batf3* removed the DC1 population, strongly reduced CCR7+DCs (13-fold), and XCR1+DCs (5-fold). The DC2 and pDC populations were unaltered in the *Batf3* knockout TdLN-c (figure 5F). There was no difference in mRNA expression of *H2-k1* between DCs from TdLN or TdLN-c (online supplemental figure 5F).

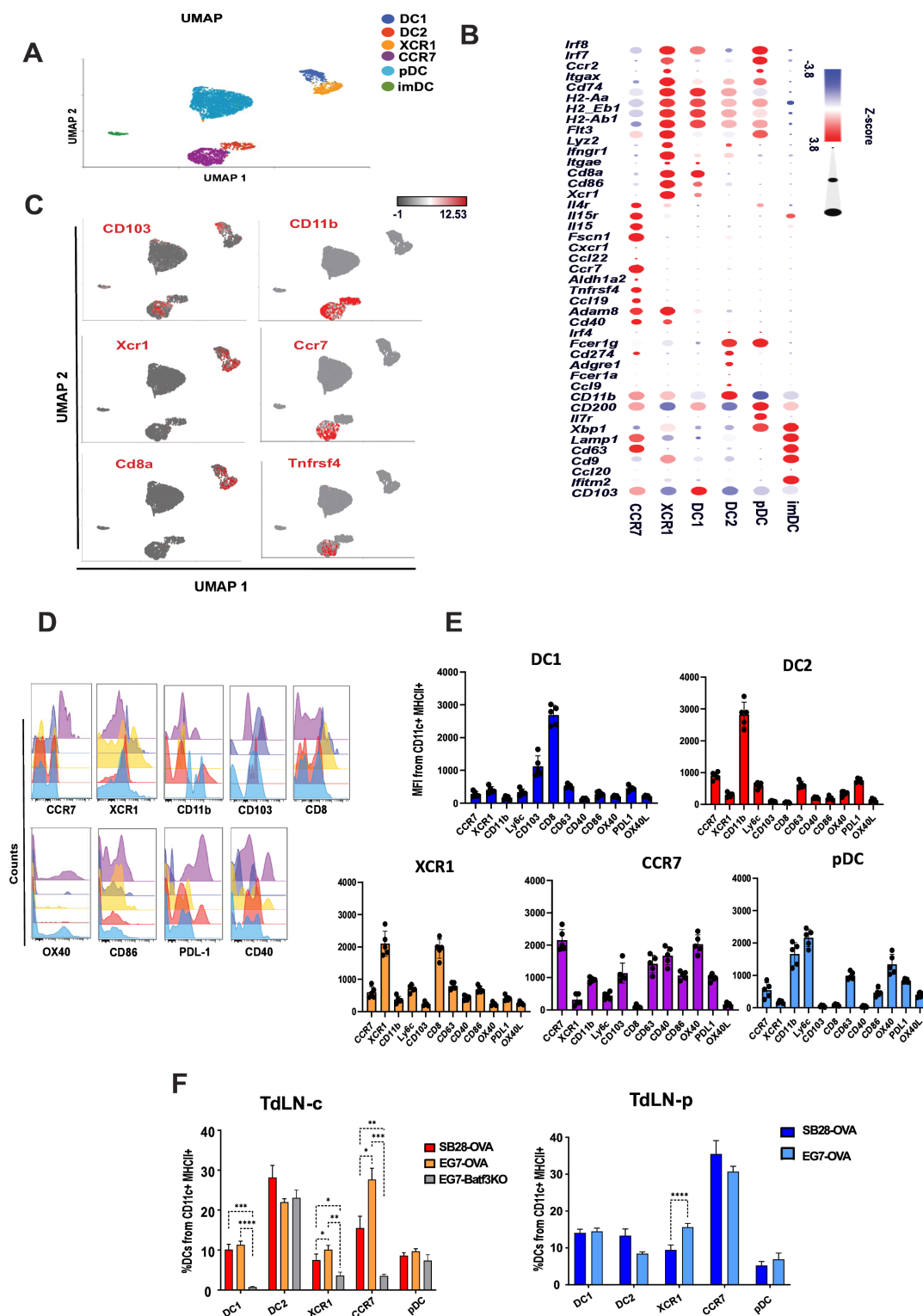


Figure 5 Profiles of dendritic cell (DC) subpopulations in tumor-draining lymph nodes (TdLNs) vary based on the tumor site and type. SB28-OVA or EG7-OVA was implanted i.c. or s.c. Mice were sacrificed on day 12 after tumor inoculation. DCs TdLN were enriched for scRNA-seq analysis or flow cytometry analysis. (A) Uniform manifold approximation and projection (UMAP) of the scRNA-seq profiles of 9904 TdLN cells. (B) Bubble heatmap of genes upregulated in each DC cluster; values are presented as averaged Z-scores. Statistical analysis involved filtering genes based on a false discovery rate (FDR) cut-off of <0.05 . FDR (Benjamini-Hochberg adjustment) was calculated from the p values obtained using ANOVA. (C) UMAP expression of genes associated with DC1 (*Cd8a*, *CD103*, and *Xcr1*). Migratory DC (*Ccr7*), DC2 (*CD11b*), and OX40 (*Tnfrsf4*). (D, E) Display the median fluorescence intensity (MFI) data for the different markers were calculated using flow cytometry. (F) TdLN DCs from SB28-OVA or EG7-OVA mice were obtained on day 12, and the percentage of the DC population was calculated. Bar graphs show the mean \pm SD; two-way ANOVA with Tukey's correction: * $p < 0.05$, ** $p < 0.01$, *** $p < 0.001$, **** $p < 0.0001$. ANOVA, analysis of variance; i.c., intracranially; s.c., subcutaneously.

These findings indicate that six subpopulations in TdLN-c and-p and DC2-c showed increased TdLN-c in both tumor models, whereas XCR1+DC and CCR7+DC depended on the tumor model.

CCR7+, OX40+ DCs are associated with the impact of OX40 agonist treatment

The CCR7+DC population showed the highest signal for antigen uptake and processing ex vivo, and CCR7+DC-p was slightly more capable of antigen uptake and processing than the DC-c population. DC2 had the second highest signal for antigen uptake and processing with a slightly higher signal in DC-c than DC-p (figure 6A,B). Furthermore, agonistic OX40 treatment significantly increased CD40 and CD86 expression and reduced PD-L1 expression in CCR7+DC, with no notable changes in the other DC subpopulations (figure 6C–E and online supplemental figure 6A). OX40L is critical in promoting T-cell survival and activation via interaction with OX40.³⁶ We evaluated the expression of OX40L on DCs and found that it was expressed across all DC subtypes in TILs but not in TdLNs, consistent with a recent report showing that OX40 is expressed in CCR7+DCs in the TIME and is gradually lost in trafficking to the TdLN.³⁷ The expression of OX40L in DCs was induced on ex vivo stimulation with the OVA antigen (online supplemental figure 6B). To address the function of OX40 and OX40L in DCs, ex vivo cultures of DCs were treated with an OX40 agonist or OX40L blocking antibody and co-cultured with OT cells. Stimulation of DCs with OX40 using an agonist prevented Treg induction, while blocking OX40L reduced the cytotoxic profile of CD8+T cells (online supplemental figure 6C).

We characterized the double-positive CCR7+OX40+ DC population using flow cytometry. The fraction of CCR7+OX40+ DCs was more than double in SB28-OVA DC-p, EG7-OVA DC-c, and DC-p than in SB28 DC-c (figure 6F). Furthermore, the CCR7+ population is linked to LAMP3+ expression and is associated with mregDCs (CD200+CD40+CCR7+) in TIME.¹⁵ We evaluated the presence of LAMP3+DC and OX40 staining in the TIME and observed a higher prevalence in EG7-OVA than in SB28. There were few LAMP3+OX40+ double-positive cells in the TIME of EG7 tumors in *Batf3* knockout mice (figure 6G,H). Given the high numbers of CCR7+OX40+ DCs in TILs and LAMP3+OX40+ in the TIME, we assessed the antitumor response in the EG7 model. First, without treatment, the absence of *Batf3* resulted in shortened survival in the brain tumor model using EG7-OVA cells, indicating the essential role of DC1, XCR1+, and/or CCR7+DCs, given that these populations were reduced in the *Batf3* knockout model (figures 5F and 6I). There was an over 12-fold reduction in CCR7+OX40+ DCs in TdLN-c in *Batf3* knockout mice as compared with the wild type (figure 6F and online supplemental figure 5D). The mice were treated with an OX40 agonist, which elicited a robust response and led to a survival rate of 71%. The effect of OX40 agonist treatment depended on *Batf3*

and a reduction in CCR7+OX40+ DCs after OX40 agonist treatment in TdLN-c and TIME was observed (online supplemental figure 6D,E).

To assess the role of TdLN in therapy response, lymphocyte traffic was blocked by FTY720³⁸ (online supplemental figure 6F,G), which significantly reduced the frequency of circulating CD3+T cells in the blood. Mice injected with FTY720 failed to respond to the OX40 agonist treatment (figure 6J).

These findings suggest that CCR7+OX40+ DCs are essential for mounting an OX40-dependent immune response in brain tumors. Our data are consistent with OX40L signaling from DCs to T cells in the TIME, a potentially important mechanism, besides the direct stimulation of OX40 on DCs and T cells. Finally, our data indicated that TdLN DCs orchestrate the immune response against brain tumors.

DISCUSSION

Stimulating OX40 enhances the survival of glioma-bearing mice, particularly when combined with vaccination using irradiated tumors or GM-CSF-expressing cells, supporting the importance of DCs and OX40 signaling in this context.^{39,40} We expanded on these findings by assessing the tolerogenic functions of DC-c compared with DC-p by analyzing DC subpopulations ex vivo and in vivo to elucidate the possible mechanisms of action of OX40 agonist treatment in brain tumors.

First, these diverse models showed that TdLN-c exhibited a tolerogenic response, characterized by increased Tregs and poor cytotoxic T-cell activation. Using ex vivo cultures, we demonstrated the direct effect of TdLN DCs on Treg generation. The tolerogenic DC-c response could be reversed by agonistic OX40 treatment, resulting in T-cell proliferation and reduced Treg development, in line with previous data.³³

Second, the OX40 agonist induced CD40 and CD86 expression, promoted antigen presentation, and reduced PD-L1 expression in DCs in vivo. OX40 stimulation affected CCR7+DCs ex vivo but not other subpopulations. Moreover, blocking OX40L on DCs ex vivo increases Tregs and reduces cytotoxic T cells, suggesting a direct effect of OX40L on T cells mediated by DCs. OX40L was highly expressed in CCR7+DCs and pDC. *Batf3* knockout mice had intact pDC and DC2 populations, whereas there was virtually no DC1, strongly reduced CCR7+, and diminished XCR1+DCs. There was a fivefold reduction in CCR7+OX40+ DCs in the *Batf3* knockout model compared with SB28. Furthermore, this reduction was even more pronounced when compared with the EG7 model, showing a 12-fold decrease, suggesting a central role for CCR7+OX40+ OX40L in the effect of OX40 agonist in the brain tumor models, as no effect of OX40 agonist was observed in *Batf3* knockout mice.

We could not establish CCR7 as a reliable marker using tissue sections; therefore, we used LAMP3+OX40+ double staining as a surrogate and observed a similar correlation

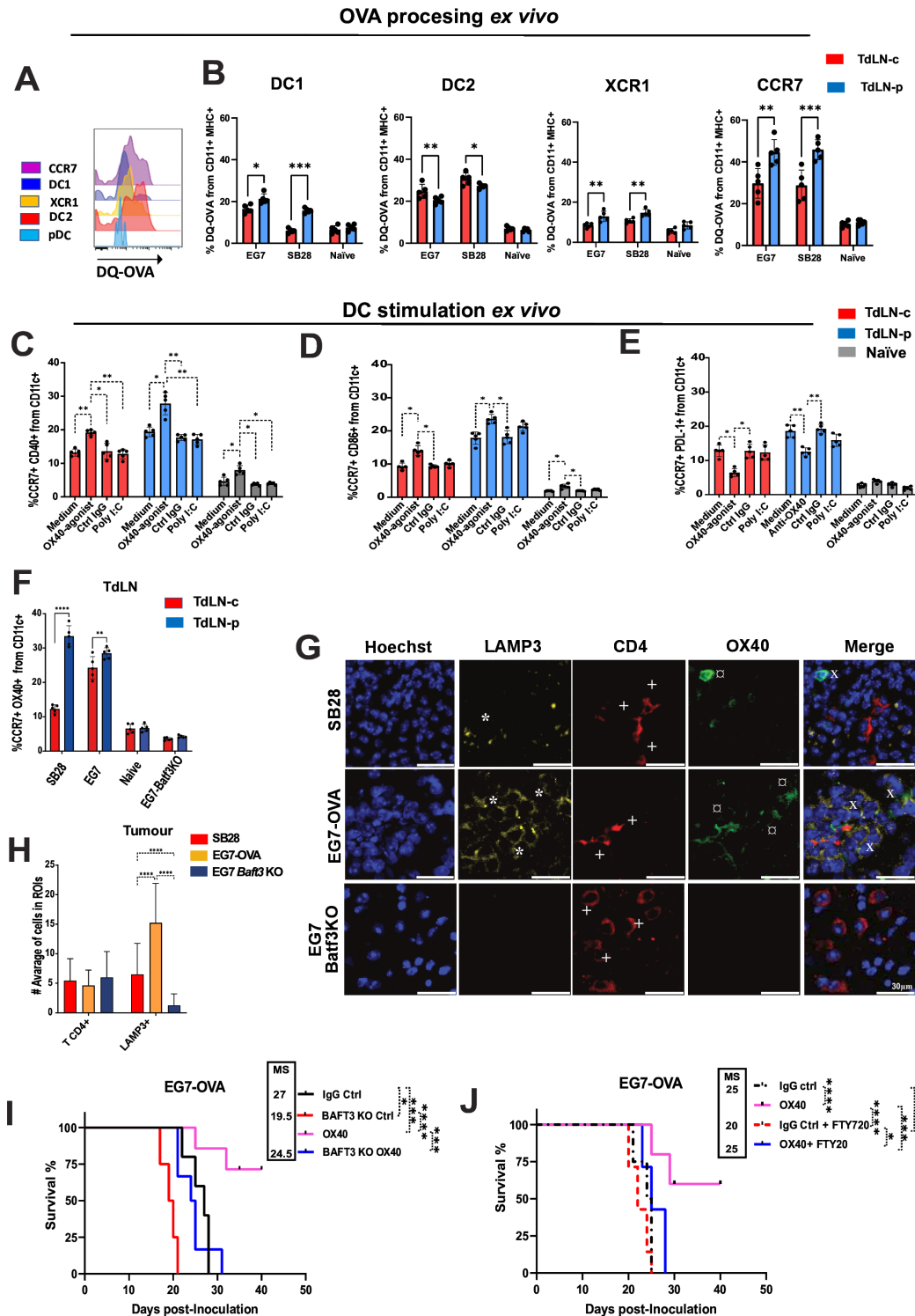


Figure 6 CCR7+OX40+ dendritic cells (DCs) in cervical lymph nodes correlate with anti-OX40 agonist immunotherapy. DCs from TdLNs were isolated and cultured in the presence of the labeled peptide DQ-OVA, which allowed for quantification of antigen uptake, processing, and presentation. (A, B) Representative histograms and percentages of DQ-OVA signals in different DC populations. (C) DCs from TdLN were cultured as in (A) and incubated in the presence of anti-OX40 agonist, Poly-I:C or IgG control. The percentages of CD40 (C), CD86 (D), and PDL-1 (E) were calculated. (F) The percentage of CCR7+OX40+ DCs was calculated from TdLNs harvested 12 days post-tumor inoculation. (G) Representative immunofluorescence staining images of brain sections showing LAMP3+ (*), CD4+ (+), and OX40+ (□). (H) The graph shows the average number of positive cells across different regions of interest (ROIs, n=392). (I, J) Kaplan-Meier survival curves of EG7-OVA tumor-bearing mice treated with agonistic OX40 antibody or IgG control, either alone or combined with FTY720, were analyzed using the log-rank test (n=5–7 mice/group test). Statistical analyses were conducted using the Mann-Whitney U test. Bar graphs show the mean±SD; two-way ANOVA with Tukey's correction: *p<0.05, **p<0.01, ***p<0.001, ****p<0.0001. ANOVA, analysis of variance TdLNs, tumor-draining lymph nodes.

of more LAMP3+OX40+ cells in the TIME in EG7 to SB28 and loss of staining in *Batf3* knockout. If there is a specific effect of OX40L on DCs, it is likely to occur in the TIME, as OX40L is expressed in the TIME and ex vivo, but not in TdLNs. This is consistent with the findings of a recent study where CCR7+DC were tracked in tumor models in vivo and expressed OX40L in the TIME but not in the TdLN.³⁷ We show that the effect of the OX40 agonist was also blocked by FTY720-mediated inhibition of lymphocyte trafficking, indicating either a role for OX40 stimulation in the TdLN or a need for SIP-mediated lymphocyte mobilization for the effect of the OX40 agonist.

Third, we characterized the subpopulations of DCs derived from TdLN-c and TdLN-p using scRNA sequencing. DC subpopulations have been identified intratumorally and in TdLNs as crucial elements for regulating immune response.^{7 10 15 41 42} Using scRNA-seq, we identified six clusters of TdLN-c and TdLN-p. There were no major differences in mRNA expression that suggested a new subpopulation in TdLN-c or TdLN-p. The six subpopulations express well-established markers for DC1, DC2, and pDC.⁴³ We identified three clusters we termed XCR1+, CCR7+, and imDCs. The similarities between these clusters and other subpopulations of previously defined DCs were not obvious, possibly because different platforms and tissue sources were used. For instance, DC3 cells have been characterized by the expression of *Lyz2*, *Flt3*, and *Ccr2*, as expressed by the *Xcr1*+ DC cluster, but not *Cd8a*, *Irf8*, or *Xcr1*.⁴⁴ mregDC cells have been reported to express *Ccr7*, *Il4r*, *Ccl19*, *Tnfrsf4*, and *Aldh1a2*,^{15 45 46} as well as XCR1.¹⁵ In GBM, intratumoral migratory DCs, as defined by Pombo Antunes *et al*, show high expression of *Cd274*, *Cd200*, and *Cd63*, similar to *Ccr7*+DCs.⁴² *Irf7* was consistently overexpressed in DC from TdLN-c, irrespective of DC subtype. In addition, *Ifitm3* and *Tmem173* were overexpressed in CCR7+DC, suggesting that type I interferon responses may be altered in response to brain tumors compared with peripheral tumors.

The upregulated *Tmem173*, encoding the stimulator of interferon genes (STING), initiates type I interferon signaling via the cGAS-STING pathway on DNA detection.⁴⁷ Notably, STING is present in human GBM samples, and the activation of the pathway result in the robust action of the innate immune system and regression of experimental gliomas.⁴⁸

This study had some limitations. Mouse models have significantly advanced our understanding of GBM biology and the development of novel therapeutic strategies. However, each model has unique characteristics that influence the validity and translatability of experimental results. The most widely used mouse glioma model, GL261, responds to ICI and has a high neoantigen load and, compared with SB28, higher infiltration of cDC2 and T cells.^{23 49} Both models exhibited a high number of tumor-associated macrophages (TAMs), and the TAM:T-cell ratio was 62:1 in SB28 and 4:1 in GL261.²³ However, other factors, such as tumor inflammation, are also important in determining the response to ICI.⁵⁰ We

used SB28 for its relative similarity to GBM in terms of TIME composition and lack of response to ICI. To study the non-glioma aspects of brain tumors, we used the lymphoma model EG7 to obtain different TIME triggered by a distinct cancer type that can engage the brain. However, some aspects of disease biology are not optimally reflected in these models.

We did not determine whether there was a DC subtype that was more immunoregulatory than the other subtypes. scRNA sequencing separates DC subtypes, but gives no spatial resolution in the tumor tissue. It is difficult to isolate and assess the functional properties of corresponding subpopulations ex vivo. In gliomas, myeloid cells are the most prevalent non-malignant cell type, comprising up to half of the tumor and significantly influencing T-cell infiltration and function. Myeloid compartments are conventionally classified into microglia, macrophages, monocytes, cDCs, and neutrophils. This work focused on DC subsets, but other immune cells, especially other myeloid cell subsets such as TAMs and myeloid-derived suppressor cells, also have important roles in shaping the brain tumor TIME.^{23 42} Understanding the full interplay of myeloid subsets is important for understanding the GBM TIME. With a few samples for scRNA analysis, differences with smaller effect sizes between TdLN-c and TdLN-p might have been overlooked. Pharmacological blockage of LN trafficking suggested a role for TdLN in the immune response to brain tumors; however, we could not pinpoint the exact location(s) of OX40 agonist action (in TdLN or TIME) or whether the primary effect is on DCs or T cells. Future studies using other brain tumor models and expanding scRNA profiling are warranted to determine the generalizability of these findings and to identify more genes associated with TdLN-c.

In conclusion, brain TdLN DCs display a unique marker expression and default regulatory program influenced by brain tumor type. The OX40 agonist treatment directly affected the activation of CCR7+OX40+ OX40L+DCs. Blocking OX40L on DCs or stimulating OX40 blocks or promotes cytotoxic T cells and reduces Tregs. Reprogramming of CCR7+OX40+ DC-c through OX40 stimulation could be explored with other immunomodulators for antitumor responses in CNS tumors.

X Oscar Badillo-Godinez @oscar_daniel and Hitesh Bhagavanbhai Mangukhiya @hitmangukhiya

Acknowledgements We would like to express our gratitude to Professors Anna Dimberg and Magnus Essand from IGP, Uppsala University, for their insightful feedback on this work. We thank Jenifer Lundqvist for technical assistance and the BioVis Core Facility at Uppsala University for assistance with flow cytometry. This work was supported by grants from the Swedish Cancer Society and Lions Cancer Foundation. Sequencing was performed by the SNP&SEQ Technology Platform in Uppsala, which is part of the National Genomics Infrastructure (NGI) Sweden and Science for Life Laboratory. The SNP&SEQ Platform is also supported by the Swedish Research Council and the Knut and Alice Wallenberg Foundation.

Contributors OB-G and MH designed the study and wrote the manuscript. OB-G, LH, SK, and JN performed the experiments and analyzed the data. MR contributed to the cytometry and single-cell RNA sequencing experiments and analysis. HBM and SN contributed to the staining and immunofluorescence analysis of the TIME. MH is the guarantor of this work, accepts full responsibility for the finished study,

had access to the data, and controlled the decision to publish. All authors edited, reviewed, and approved the manuscript.

Funding This study was funded by Cancerfonden, Lions Cancer Foundation, and Swedish Cancer Society.

Competing interests None declared.

Patient consent for publication Not applicable.

Provenance and peer review Not commissioned; externally peer reviewed.

Data availability statement Data are available on reasonable request.

Supplemental material This content has been supplied by the author(s). It has not been vetted by BMJ Publishing Group Limited (BMJ) and may not have been peer-reviewed. Any opinions or recommendations discussed are solely those of the author(s) and are not endorsed by BMJ. BMJ disclaims all liability and responsibility arising from any reliance placed on the content. Where the content includes any translated material, BMJ does not warrant the accuracy and reliability of the translations (including but not limited to local regulations, clinical guidelines, terminology, drug names and drug dosages), and is not responsible for any error and/or omissions arising from translation and adaptation or otherwise.

Open access This is an open access article distributed in accordance with the Creative Commons Attribution Non Commercial (CC BY-NC 4.0) license, which permits others to distribute, remix, adapt, build upon this work non-commercially, and license their derivative works on different terms, provided the original work is properly cited, appropriate credit is given, any changes made indicated, and the use is non-commercial. See <http://creativecommons.org/licenses/by-nc/4.0/>.

ORCID iDs

Oscar Badillo-Godinez <http://orcid.org/0000-0002-3840-9448>

Hitesh Bhagavanbhai Mangukiyi <http://orcid.org/0000-0002-8460-4850>

REFERENCES

- Mohme M, Neidert MC. Tumor-Specific T Cell Activation in Malignant Brain Tumors. *Front Immunol* 2020;11:205.
- Sampson JH, Gunn MD, Fecci PE, et al. Brain immunology and immunotherapy in brain tumours. *Nat Rev Cancer* 2020;20:12–25.
- Tawbi H, To TM, Bartley K, et al. Treatment patterns and clinical outcomes for patients with melanoma and central nervous system metastases: A real-world study. *Cancer Med* 2022;11:139–50.
- Zhang Y, Zhang Z. The history and advances in cancer immunotherapy: understanding the characteristics of tumor-infiltrating immune cells and their therapeutic implications. *Cell Mol Immunol* 2020;17:807–21.
- Tawbi HA, Forsyth PA, Algazi A, et al. Combined Nivolumab and Ipilimumab in Melanoma Metastatic to the Brain. *N Engl J Med* 2018;379:722–30.
- Hu X, Yu H, Zheng Y, et al. Immune Checkpoint Inhibitors and Survival Outcomes in Brain Metastasis: A Time Series-Based Meta-Analysis. *Front Oncol* 2020;10.
- Del Prete A, Salvi V, Soriani A, et al. Dendritic cell subsets in cancer immunity and tumor antigen sensing. *Cell Mol Immunol* 2023;20:432–47.
- Srivastava S, Jackson C, Kim T, et al. A Characterization of Dendritic Cells and Their Role in Immunotherapy in Glioblastoma: From Preclinical Studies to Clinical Trials. *Cancers (Basel)* 2019;11:537.
- Gardner A, Ruffell B. Dendritic Cells and Cancer Immunity. *Trends Immunol* 2016;37:855–65.
- Zhang Q, He Y, Luo N, et al. Landscape and Dynamics of Single Immune Cells in Hepatocellular Carcinoma. *Cell* 2019;179:829–45.
- Nirschl CJ, Suárez-Fariñas M, Izar B, et al. IFN γ -Dependent Tissue-Immune Homeostasis Is Co-opted in the Tumor Microenvironment. *Cell* 2017;170:127–41.
- Cillo AR, Kürten CHL, Tabib T, et al. Immune Landscape of Viral- and Carcinogen-Driven Head and Neck Cancer. *Immunity* 2020;52:183–99.
- Ji AL, Rubin AJ, Thrane K, et al. Multimodal Analysis of Composition and Spatial Architecture in Human Squamous Cell Carcinoma. *Cell* 2020;182:497–514.
- Zilionis R, Engblom C, Pfirschke C, et al. Single-Cell Transcriptomics of Human and Mouse Lung Cancers Reveals Conserved Myeloid Populations across Individuals and Species. *Immunity* 2019;50:1317–34.
- Maier B, Leader AM, Chen ST, et al. A conserved dendritic-cell regulatory program limits antitumour immunity. *Nature New Biol* 2020;580:257–62.
- Gerhard GM, Bill R, Messemaker M, et al. Tumor-infiltrating dendritic cell states are conserved across solid human cancers. *J Exp Med* 2021;218:e20200264.
- Zhang L, Li Z, Skrzypczynska KM, et al. Single-Cell Analyses Inform Mechanisms of Myeloid-Targeted Therapies in Colon Cancer. *Cell* 2020;181:442–59.
- Lee AH, Sun L, Mochizuki AY, et al. Neoadjuvant PD-1 blockade induces T cell and cDC1 activation but fails to overcome the immunosuppressive tumor associated macrophages in recurrent glioblastoma. *Nat Commun* 2021;12:6938.
- Friedrich M, Hahn M, Michel J, et al. Dysfunctional dendritic cells limit antigen-specific T cell response in glioma. *Neuro Oncol* 2023;25:263–76.
- Liau LM, Ashkan K, Brem S, et al. Association of Autologous Tumor Lysate-Loaded Dendritic Cell Vaccination With Extension of Survival Among Patients With Newly Diagnosed and Recurrent Glioblastoma: A Phase 3 Prospective Externally Controlled Cohort Trial. *JAMA Oncol* 2023;9:112–21.
- Smalley I, Chen Z, Phadke M, et al. Single-Cell Characterization of the Immune Microenvironment of Melanoma Brain and Leptomeningeal Metastases. *Clin Cancer Res* 2021;27:4109–25.
- Mellman I, Chen DS, Powles T, et al. The cancer-immunity cycle: Indication, genotype, and immunotype. *Immunity* 2023;56:2188–205.
- Simonds EF, Lu ED, Badillo O, et al. Deep immune profiling reveals targetable mechanisms of immune evasion in immune checkpoint inhibitor-refractory glioblastoma. *J Immunother Cancer* 2021;9:e002181.
- Kilkenny C, Browne WJ, Cuthill IC, et al. Improving bioscience research reporting: the ARRIVE guidelines for reporting animal research. *PLoS Biol* 2010;8:e1000412.
- Ramachandran M, Vaccaro A, van de Walle T, et al. Tailoring vascular phenotype through AAV therapy promotes anti-tumor immunity in glioma. *Cancer Cell* 2023;41:1134–51.
- Renkema KR, Huggins MA, Borges da Silva H, et al. KLRG1⁺ Memory CD8 T Cells Combine Properties of Short-Lived Effectors and Long-Lived Memory. *J Immunol* 2020;205:1059–69.
- Sánchez-Paulete AR, Teixeira Á, Quetglas JL, et al. Intratumoral Immunotherapy with XCL1 and sFlt3L Encoded in Recombinant Semliki Forest Virus-Derived Vectors Fosters Dendritic Cell-Mediated T-cell Cross-Priming. *Cancer Res* 2018;78:6643–54.
- Roberts EW, Broz ML, Binnewies M, et al. Critical Role for CD103(+)/CD141(+) Dendritic Cells Bearing CCR7 for Tumor Antigen Trafficking and Priming of T Cell Immunity in Melanoma. *Cancer Cell* 2016;30:324–36.
- Salmon H, Idoyaga J, Rahman A, et al. Expansion and Activation of CD103(+) Dendritic Cell Progenitors at the Tumor Site Enhances Tumor Responses to Therapeutic PD-L1 and BRAF Inhibition. *Immunity* 2016;44:924–38.
- Balan S, Saxena M, Bhardwaj N. Dendritic cell subsets and locations. *Int Rev Cell Mol Biol* 2019;348:1–68.
- Yang F, He Z, Duan H, et al. Synergistic immunotherapy of glioblastoma by dual targeting of IL-6 and CD40. *Nat Commun* 2021;12.
- Xu S, Tang L, Li X, et al. Immunotherapy for glioma: Current management and future application. *Cancer Lett* 2020;476:1–12.
- Deng J, Zhao S, Zhang X, et al. OX40 (CD134) and OX40 ligand, important immune checkpoints in cancer. *Oncotargets Ther* 2019;12:7347–53.
- Simonetta F, Chiali A, Cordier C, et al. Increased CD127 expression on activated FOXP3+CD4+ regulatory T cells. *Eur J Immunol* 2010;40:2528–38.
- Giles AJ, Hutchinson M-KND, Sonnemann HM, et al. Dexamethasone-induced immunosuppression: mechanisms and implications for immunotherapy. *J Immunother Cancer* 2018;6:51.
- Croft M. The role of TNF superfamily members in T-cell function and diseases. *Nat Rev Immunol* 2009;9:271–85.
- Lee CYC, Kennedy BC, Richoz N, et al. Tumour-retained activated CCR7⁺ dendritic cells are heterogeneous and regulate local antitumour cytolytic activity. *Nat Commun* 2024;15:682.
- Jiang X, Wang J, Zheng X, et al. Intratumoral administration of STING-activating nanovaccine enhances T cell immunotherapy. *J Immunother Cancer* 2022;10:e003960.
- Murphy KA, Lechner MG, Popescu FE, et al. An in vivo immunotherapy screen of costimulatory molecules identifies Fc-OX40L as a potent reagent for the treatment of established murine gliomas. *Clin Cancer Res* 2012;18:4657–68.
- Jahan N, Talat H, Curry WT. Agonist OX40 immunotherapy improves survival in glioma-bearing mice and is complementary with vaccination with irradiated GM-CSF-expressing tumor cells. *Neuro Oncol* 2018;20:44–54.

- 41 Magen A, Hamon P, Fiaschi N, *et al.* Intratumoral dendritic cell-CD4⁺ T helper cell niches enable CD8⁺ T cell differentiation following PD-1 blockade in hepatocellular carcinoma. *Nat Med* 2023;29:1389–99.
- 42 Pombo Antunes AR, Scheyltjens I, Lodi F, *et al.* Single-cell profiling of myeloid cells in glioblastoma across species and disease stage reveals macrophage competition and specialization. *Nat Neurosci* 2021;24:595–610.
- 43 Duluc D, Sisirak V. Origin, phenotype, and function of mouse dendritic cell subsets. In: Sisirak V, ed. *Dendritic Cells*. New York: Springer US, 2023: 3–16.
- 44 Liu Z, Wang H, Li Z, *et al.* Dendritic cell type 3 arises from Ly6C⁺ monocyte-dendritic cell progenitors. *Immunity* 2023;56:1761–77.
- 45 Ziblat A, Horton BL, Higgs EF, *et al.* Batf3⁺ DCs and the 4-1BB/4-1BBL axis are required at the effector phase in the tumor microenvironment for PD-1/PD-L1 blockade efficacy. *Cell Rep* 2024;43:114141.
- 46 You S, Li S, Zeng L, *et al.* Lymphatic-localized Treg-mregDC crosstalk limits antigen trafficking and restrains anti-tumor immunity. *Cancer Cell* 2024;42:1415–33.
- 47 Cai X, Chiu Y-H, Chen ZJ. The cGAS-cGAMP-STING pathway of cytosolic DNA sensing and signaling. *Mol Cell* 2014;54:289–96.
- 48 Berger G, Knelson EH, Jimenez-Macias JL, *et al.* STING activation promotes robust immune response and NK cell-mediated tumor regression in glioblastoma models. *Proc Natl Acad Sci U S A* 2022;119:e2111003119.
- 49 Reardon DA, Gokhale PC, Klein SR, *et al.* Glioblastoma Eradication Following Immune Checkpoint Blockade in an Orthotopic, Immunocompetent Model. *Cancer Immunol Res* 2016;4:124–35.
- 50 Gromeier M, Brown MC, Zhang G, *et al.* Very low mutation burden is a feature of inflamed recurrent glioblastomas responsive to cancer immunotherapy. *Nat Commun* 2021;12:352.